

Article

Arsenite to Arsenate Oxidation and Water Disinfection via Solar Heterogeneous Photocatalysis: A Kinetic and Statistical Approach

Felipe de J. Silerio-Vázquez ¹, Cynthia M. Núñez-Núñez ², José B. Proal-Nájera ^{3,*}
and María T. Alarcón-Herrera ^{1,*}

¹ Departamento de Ingeniería Sustentable, Centro de Investigación en Materiales Avanzados, S.C. Calle CIMAV 110, Colonia 15 de Mayo, Durango 34147, Mexico

² Ingeniería en Tecnología Ambiental, Universidad Politécnica de Durango, Carretera Durango-México km 9.5, Durango 34300, Mexico

³ CIIDIR-Durango, Instituto Politécnico Nacional, Calle Sigma 119, Fraccionamiento 20 de Noviembre II, Durango 34220, Mexico

* Correspondence: jproal@ipn.mx (J.B.P.-N.); teresa.alarcon@cimav.edu.mx (M.T.A.-H.);
Tel.: +52-618-1341781 (J.B.P.-N.); +52-614-4394896 (M.T.A.-H.)



Citation: Silerio-Vázquez, F.d.J.; Núñez-Núñez, C.M.; Proal-Nájera, J.B.; Alarcón-Herrera, M.T. Arsenite to Arsenate Oxidation and Water Disinfection via Solar Heterogeneous Photocatalysis: A Kinetic and Statistical Approach. *Water* **2022**, *14*, 2450. <https://doi.org/10.3390/w14152450>

Academic Editors: Antonio Zuorro, Zacharias Frontistis, José A. Peres, Gassan Hodaifa, Joaquín R. Dominguez and Juan García Rodríguez

Received: 6 July 2022

Accepted: 5 August 2022

Published: 8 August 2022

Publisher's Note: MDPI stays neutral with regard to jurisdictional claims in published maps and institutional affiliations.



Copyright: © 2022 by the authors. Licensee MDPI, Basel, Switzerland. This article is an open access article distributed under the terms and conditions of the Creative Commons Attribution (CC BY) license (<https://creativecommons.org/licenses/by/4.0/>).

Abstract: Arsenic (As) poses a threat to human health. In 2014, more than 200 million people faced arsenic exposure through drinking water, as estimated by the World Health Organization. Additionally, it is estimated that drinking water with proper microbiological quality is unavailable for more than 1 billion people. The present work analyzed a solar heterogeneous photocatalytic (HP) process for arsenite (As^{III}) oxidation and coliform disinfection from a real groundwater matrix employing two reactors, a flat plate reactor (FPR) and a compound parabolic collector (CPC), with and without added hydrogen peroxide (H₂O₂). The pseudo first-order reaction model fitted well to the As oxidation data. The treatments FPR-HP + H₂O₂ and CPC-HP + H₂O₂ yielded the best oxidation rates, which were over 90%. These treatments also exhibited the highest reaction rate constants, $6.7 \times 10^{-3} \text{ min}^{-1}$ and $6.8 \times 10^{-3} \text{ min}^{-1}$, respectively. The arsenic removal rates via chemical precipitation reached 98.6% and 98.7% for these treatments. Additionally, no coliforms were detected at the end of the process. The collector area per order (A_{CO}) for HP treatments was on average 75% more efficient than photooxidation (PO) treatments. The effects of the process independent variables, H₂O₂ addition, and light irradiation were statistically significant for the As^{III} oxidation reaction rate ($p < 0.05$).

Keywords: groundwater; real water matrix; reactor prototype; arsenic speciation; collector area per order

1. Introduction

The abundance of arsenic (As) in the Earth's crust is around 1.5–3 mg/kg, making it the 20th most abundant element and a component of more than 245 minerals [1]. When the groundwater's pH and bicarbonate anion (HCO₃[−]) concentration are high, As is easily dissolved and passes to the groundwater cycle [2]. As toxicity affects all body systems, causing both acute and chronic poisoning [3]. Acute exposure is rare and happens mostly with exposure to arsenite (As^{III}) than arsenate (As^V) [4]. Long-term exposure leads to a variety of illnesses known as arsenicosis [5], which includes skin, bladder, kidney, and lung cancer, along with black foot disease [6]. As^{III} is more toxic than As^V [7] and also harder to remove from water [8].

With nearly 1 billion people exposed to arsenic by food, and more than 200 million people exposed to it via drinking water [9–11], As is a serious threat to the physical, social, and economic well-being of people, affecting especially the population of developing

countries [12]. Countries affected by high arsenic concentrations in groundwater include Argentina, Australia, Bangladesh, China, Chile, Mexico, India, New Zealand, Nepal, USA, Vietnam, and Taiwan [13].

In addition, the typical and harmful pollutants in developing countries are of biological origin, as diseases present in almost 50% of their populations are associated with water, both for supply and sanitation [14]. Worldwide, according to estimations, safe drinking water is unavailable for 1.1 billion people; water scarcity is suffered by 2.7 billion people, and 5 million people die each year due to waterborne infections [15,16]. These infections can be caused by viruses, bacteria, or protozoa [17].

The World Health Organization (WHO) recommends that the As amount in water should not surpass 10 $\mu\text{g}/\text{L}$ [18]; as for microbiological water quality, the WHO recommends the use of the following microbial water quality indicators: total coliforms, thermotolerant coliforms, *Escherichia coli*, intestinal enterococci, enteric virus, and coliphage virus (none of which should be detected in drinking water) [19].

The growing population and climate change are two of the main factors that are increasing the demand for drinking water; it is then a priority to research drinking water treatments to improve processes in terms of reliability, efficiency, safeness, and ease of implementation [20]. Additionally, economic feasibility, technical viability, and environmental safeness must be complied with for a technology to be considered sustainable [21].

Recently, the scientific community has shown extensive interest in advanced oxidation processes (AOPs), considering them as the most promising technologies for the potabilization of water and the treatment of wastewater on account of the nonselectivity of reactive oxidizing species (ROS), enabling AOPs to remove pollutants, including microbes and organic and inorganic contaminants [22].

Heterogeneous photocatalysis (HP) with semiconductors (or photocatalysts) is an AOP developed in 1972 with several advantages, including its ability to use solar light and that fact that is environmentally friendly and has a relatively low cost [23–25]. When the photocatalyst is irradiated with light whose energy is higher than the photocatalyst bandgap energy level, electrons in the valence band (VB) migrate to the conduction band (CB), generating a positive hole (h^+) and an extra electron (e^-) in the VB and CB, respectively [26]. Oxygen adsorbed on the photocatalyst surface can react with e^- to form superoxide radicals ($\text{O}_2^{\bullet-}$), while water can react with h^+ to generate hydroxyl radicals (HO^\bullet) [27].

HP with titanium dioxide (TiO_2) has been investigated for As oxidation, which is a good approach as As^{III} is found as a neutral charge oxyanion in a wide pH range, and, in contrast to other oxyanions, adsorption onto metal oxides or clays is inefficient, and precipitation at near neutral pH barely occurs [28]. Although As^{V} is a triprotic acid and can be found in several forms depending of the medium pH, its removal from water is easier with processes such as chemical precipitation [29] and adsorption [30].

For the last two decades, HP has also been widely investigated for water disinfection, showing potential for treatment through oxidative stress caused by ROS, Gram positive and negative bacteria, DNA and RNA viruses, and even algae [31]. ROS can attack cell membrane components, altering cell integrity, which results in a cytoplasm leakage [32]; they can inhibit required cell activities such as protein synthesis [33]; they can also break organic covalent bonds present in biomolecules [34]. Many factors affect the efficiency of disinfection via HP, including the chemical nature and concentration of the microorganisms, time of treatment, light intensity, water matrix, deficiency of atomic ligands, surface energy level, photocatalyst properties, and solution pH [22].

One of the main drawbacks limiting commercial and industrial HP application is the lack of reactor designs efficient enough to handle large volumes of water [35]. Many types of reactors have been studied and developed, but standard procedures for scale up are still lacking; HP technology readiness level (TRL), which ranges from TRL = 1 (proof-of-concept stage) to TRL = 9 (full operational scale stage), is between TRL = 4 (lab scale validation) and TRL = 5 (ongoing pilot scale applications) [36]. Other relevant issues concerning reactor design, such as reducing photon and mass transfer limitations [37] or a thorough

understanding of heat, mass, and light transfer in the system [38], are a current research interest as are operation conditions, such as analyzing reactor performance with real water matrixes instead of synthetic water matrixes [39].

In this work, heterogeneous photocatalytic arsenic oxidation and water disinfection were explored in two types of solar reactors, a compound parabolic collector reactor (CPC) and a flat plate reactor (FPR); a real groundwater matrix was used, and coliform disinfection was also analyzed. As removal via chemical precipitation with ferric chloride (FeCl_3) was explored, following oxidation. Estimations of the collector area per order (A_{CO}) (m^2/m^3 -order) were performed for the evaluation of the area or energy requirements by every reactor. The results were also analyzed from a reaction kinetic and statistical standpoint.

2. Materials and Methods

2.1. Location and Operation Timeframe for Experiments

Experiments were carried out in the city of Durango (25.613238° N, 103.435395° W, 1900 m above sea level; Durango, Mexico), and they were performed during the summer, autumn, and winter seasons at solar noon. The city is located within the planet's sunbelt, which receives an average solar radiation in the range of $5.5 \text{ kWh}/\text{m}^2/\text{day}$ to $6.5 \text{ kWh}/\text{m}^2/\text{day}$ [40].

2.2. Photocatalytic Reactors

The experiments were performed in a CPC tubular reactor set above a compound parabolic collector; the tube was made of 3 mm thick polymethylmethacrylate (PMMA), with an inside diameter of 4.48 cm and a longitude of 90 cm; 3 mm thick PMMA plates (which served as the TiO_2 support) were placed within the tube. Galvanized iron sheet was used to make the compound parabolic reflector; commercial reflective adhesive paper was used to cover the reflector. A submersible water pump was used to feed water to the reactor from a reservoir into one end of the tube and sent it back to the reservoir using a tubing arrangement (Figure 1).

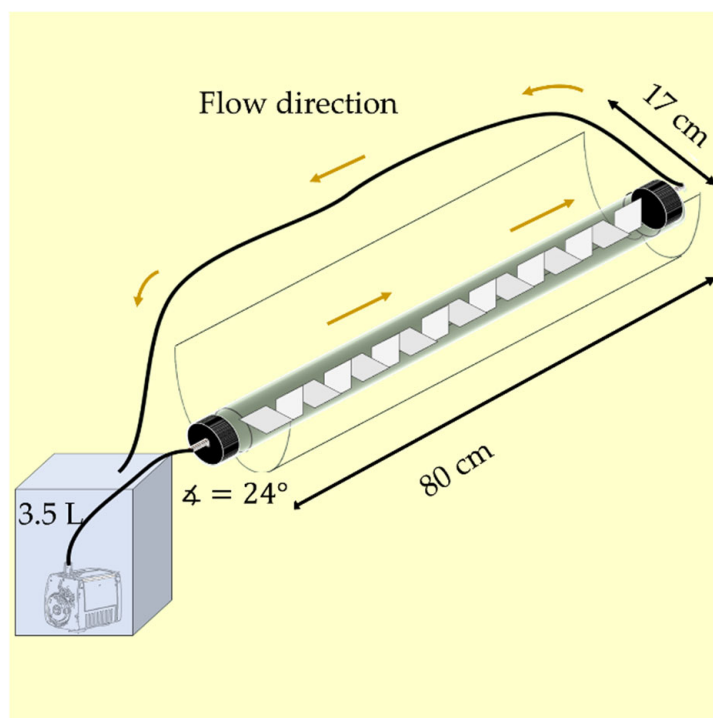


Figure 1. CPC reactor scheme.

The FPR reactor has been described in previous works [41–43], but briefly, it consisted of a PMMA compartment, with a feeding tube (with small holes separated every 0.5 cm) made of polyvinyl chloride set at the compartment's top, plus a drainage located at the compartment's bottom. The PMMA compartment was placed onto an inclinable metal assembly; reactor's drainage led to the water reservoir, which, with the help of a submersible water pump (Model H-331 BioPro, Jiangsu, China), was fed to the reactor (Figure 2). Table 1 shows additional reactor operational parameters, as reported in previous work [44].

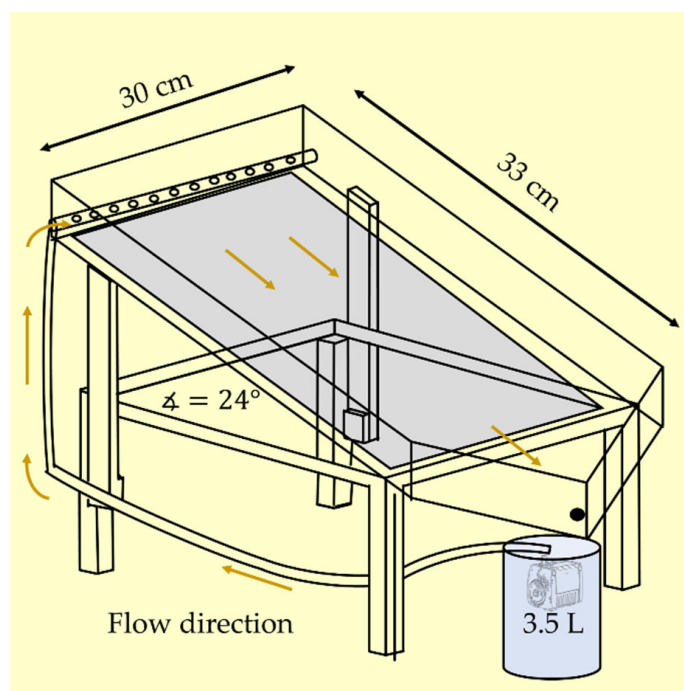


Figure 2. FPR reactor scheme.

Table 1. Operational parameters differing between reactors.

Reactor	Illuminated Net Area (m ²)	Photocatalyst Covered Area (m ²)	Volumetric Flow (m ³ /h)
FPR	0.10 ^a	0.10 ^a	0.18
CPC	1.40 ^b	0.07 ^c	1.50

Note: ^a Glass plate area, equal to area covered by photocatalyst; ^b Reactor reflector area; ^c PMMA plate area covered by photocatalyst.

In the CPC, TiO₂ (Degussa-Evonik, Essen, Germany. CAS: 13463-67-7) was immobilized on a 4.5 cm wide and 5 cm long PMMA plate, on both plate sides; sixteen plates were used. While in the FPR, a 33 cm wide and 30 cm long frosted glass plate was used as photocatalyst support. The immobilization methodology has been reported elsewhere [44].

2.3. Experimental Conditions

Each experimental run was carried out with 3.5 L of a 300 µg/L As^{III} solution prepared using sodium meta-arsenite (NaAsO₂; J.T. Baker, Radnor, PA, USA. CAS: 7784-46-5) with groundwater from a local well, which already had 46.06 µg/L of As^{III} and 5.46 µg/L of As^V; groundwater physicochemical characterization is presented in Table 2. The solution was also spiked with water from a municipal wastewater treatment plant (MWTE) to analyze As oxidation in the presence of coliforms; the initial most probable number (MPN) per 100 mL was >2419. A total of 0.358 mL from a 30% H₂O₂ (Fermont, Guadalajara, Mexico. CAS: 7722-84-1) solution was added to the water to analyze H₂O₂ addition effect. Experiments

in the dark were carried out for each experimental condition as control experiments, as well as photooxidation experiments without TiO_2 .

Table 2. Groundwater physicochemical characterization.

pH		8.52
Electrical Conductivity		548.25 $\mu\text{S}/\text{cm}$
Major ions (mg/L)		
Na^+		4.38 mg/L
K^+		53.10 mg/L
Ca^{+2}		9.87 mg/L
Mg^{+2}		60.55 mg/L
F^-		1.54 mg/L
NO_3^-		38.35 mg/L
NO_2^-		1.83 mg/L
Cl^-		26.39 mg/L
HCO_3^-		148.50 mg/L
SO_4^{-2}		59.75 mg/L
Arsenic ($\mu\text{g}/\text{L}$)		
As^{III}		46.06
As^{V}		5.46

Experiments lasted 300 min (which began 150 min before solar midday); 20 mL samples were collected at 0, 30, 60, 100, 150, 220, and 300 min to measure As^{III} oxidation during the course of the experiment. To separate As^{III} and As^{V} , for each sample, an As speciation cartridge (MetalSoft Centre, Buena Park, CA, USA) was used, according to the manufacturer's specifications [45]. A radiometer (CUV5, Kipp & Zonen, Delft, The Netherlands) was used to measure UV irradiance during experiments.

As removal was also explored. After solar treatment was over, 0.5 L samples [46] were collected to carry out chemical precipitation with an optimized dose (2.19 mg/L) of FeCl_3 (Merck, Darmstadt, Germany. CAS: 7705-08-0; determination included in Supplementary Materials), and after adding the FeCl_3 , pH was adjusted to 6.5 using hydrochloric acid (HCl; Merck, Darmstadt, Germany. CAS: 7647-01-0), and samples were taken to a jar tester machine with a rapid mixing phase of 400 rpm for 1 min, a slow mixing phase of 20 rpm for 10 min, and a settling phase for 20 min [47]. Samples were taken carefully with a micropipette from the supernatant for As quantification. Figure 3 shows a flow diagram of the process.

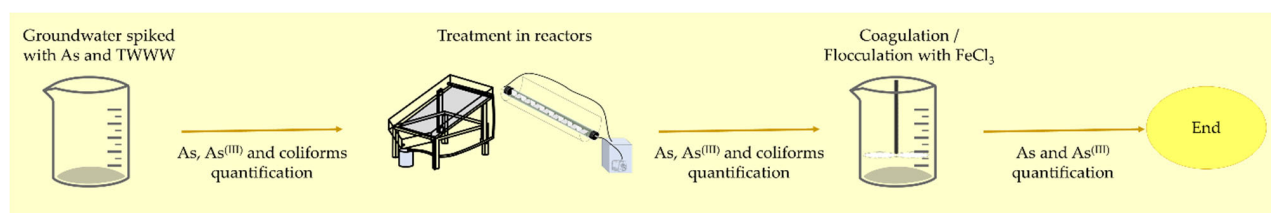


Figure 3. Process flow diagram.

Graphite furnace atomic absorption spectroscopy (GFAAS) (Avanta GBC model Xplo-rAA) was carried out to quantify As.

For the experiments exploring disinfection, coliform bacteria inactivation was assessed by MPN using the Quanty-Tray Method with defined substrate Colilert (IDEXX Laboratories, Westbrook, ME, USA) [48], which is approved by the USEPA [49]. Colilert media was added to 100 mL samples (collected at the start and end of each experiment), mixed until properly dissolved, and mixed solutions were then poured into a Quanty-Tray/2000, sealed using the Quanty-Tray sealer, then put at 35 °C for 24 h for incubation [50]. This method is based on the enzymatic activity of coliform bacteria, which metabolizes the

nutrient-indicating molecule ortho-nitrophenyl- β -D-galacto-pyranoside that turns colorless water yellow [51].

2.4. Kinetic Analysis

Scientific reports indicate that As^{III} heterogeneous photocatalytic oxidation employing supported TiO₂ follows a pseudo first-order reaction rate [52,53], which is useful to describe reactions limited by adsorption, as has been reported for heterogeneous photocatalytic reactions with TiO₂ [54,55]. As^{III} data were used to determine the K_{phC} , which was obtained by fitting the data to the pseudo first-order reaction model equation, which was obtained by established and conventional kinetics [56], as Equation (1) shows:

$$[As^{III}]_t = [As^{III}]_0 e^{-K_{phC} t}, \quad (1)$$

where $[As^{III}]_0$ is As^{III} at $t = 0$, $[As^{III}]_t$ at time t , and K_{phC} is the photocatalytic reaction rate constant. Assumptions, such as laminar flow with a Reynolds number below 1000, steady state operation, and constant fluid viscosity and density must be considered [57].

2.5. Fluence Analysis

Fluence (Q_{UV}) was calculated as indicated elsewhere [58–61] and is shown in Equation (2):

$$Q_{UV} = Q_{UV,n-1} + UV_n \cdot (t_n - t_{n-1}) \cdot \frac{A_i}{V_t}, \quad (2)$$

where the fluence is represented by Q_{UV} , the UV irradiance by UV_n , the time by t_n , the net irradiated area by A_i , and the volume by V_t . $[As^{III}]_t$ can be calculated as a function of Q_{UV} [59] employing Equation (3):

$$[As^{III}]_t = [As^{III}]_0 e^{-K_{UV} Q_{UV}}, \quad (3)$$

where K_{UV} denotes the rate constant calculated for Q_{UV} .

2.6. Collector Area per Order Determination

The collector area per order (A_{CO}) is the net area of irradiated photocatalyst needed, considering an average solar UV irradiance, to decrease a contaminant's concentration by one order of magnitude, within a unit of volume [40,62]. It can be calculated by Equation (4):

$$A_{CO} = \frac{A_c \bar{E}_s t}{V_t \log\left(\frac{[As^{III}]_0}{[As^{III}]_t}\right)}, \quad (4)$$

where the collector area per order is represented by A_{CO} , the photocatalyst covered area by A_c , the As concentration by $[As^{III}]$, the volume by V_t , the time by t , and the average solar UV irradiance by \bar{E}_s .

2.7. Experimental Design and Statistical Analysis

A full factorial 2⁵ experimental design was used to test the effects of 5 independent variables, each variable with 2 levels (for a total of 32 different experimental runs, carried out in triplicate), which can be seen in Table 3.

Table 3. Independent variables and their levels.

AOP	H ₂ O ₂	Reactor	MWTE Spike	Irradiation
Photooxidation	0 mM	CPC	0 mL	No irradiation (dark control)
Heterogeneous photocatalysis	1 mM	FPR	10 mL	Solar UV

An analysis of variance (ANOVA) was performed to determine if the effect of each one of the independent variables was significant for the result of the dependent variables [63]. Equation (5) shows the linear model used:

$$x_{ijklmn} = \bar{\mu} + AOP_i + H_2O_{2j} + R_k + MWTE_l + DC_m + Q_{UVn} + \varepsilon_{ijklmn}, \quad (5)$$

$\bar{\mu}$ is the general mean; AOP_i represents the effect of the AOP; H_2O_{2j} is H_2O_2 addition; R_k denotes the type of reactor employed; $MWTE_l$ indicates MWTE spike added; DC_m stands for DC treatment; Q_{UVn} signifies QUV, and ε_{ijklmn} is the linear model error. To perform this analysis, SAS Studio 3.8 (SAS Institute Inc., Cary, NC, USA), which is a statistical software, was used.

3. Results and Discussion

3.1. Arsenic Oxidation

Figure 4 shows As^{III} photooxidation during the experiment on both CPC and FPR. The initial As^{III} concentration was $350 \pm 2 \mu\text{g/L}$. DC experiments showed very little oxidation, which can be attributed to the effect of water and oxygen [64]. Solar photooxidation experiments showed less than 25% As^{III} oxidation. It is known that solar irradiation accelerates oxidation, which can be attributed to UV and visible light, and, as it has been reported, they also promote ROS formation in water without the need of a photocatalyst [65].

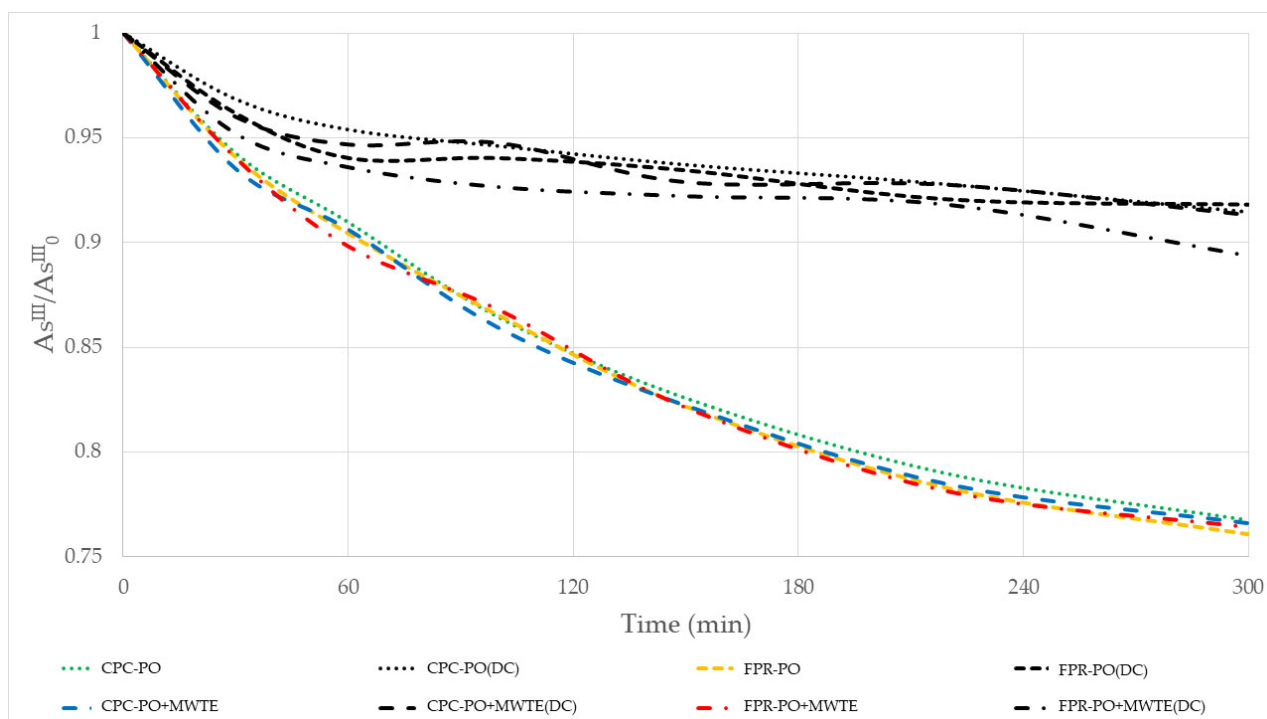


Figure 4. As^{III} photooxidation (PO) experiments carried out both in CPC and FPR, with and without MWTE spike. Experiments performed in the dark as control experiments (DC) are included as well.

Figure 5 shows also photooxidation experiments in the same treatments discussed above, but with H_2O_2 addition. The accelerated oxidation fostered by H_2O_2 observed in all cases was expected, as it has been reported that H_2O_2 is an effective oxidant in alkali conditions [66] (working solution $\text{pH} = 8.5$). Experiments under solar irradiation yielded an increased oxidation, as UV light causes H_2O_2 to undergo homolytic cleavage, generating HO^\bullet [27], whose oxidative potential of 2.73–2.8 V is only surpassed by that of fluorine [67]. Both HO^\bullet and H_2O_2 are able to promote As^{III} oxidation [68].

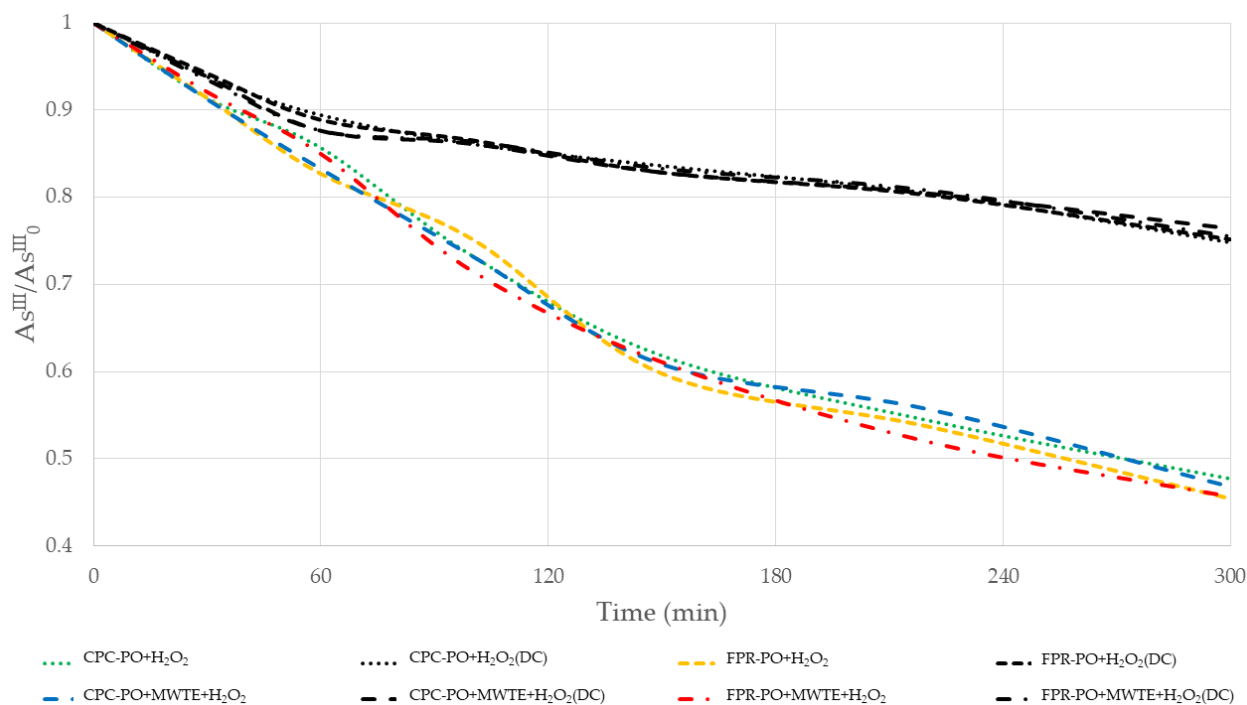


Figure 5. As^{III} photooxidation (PO) experiments carried out both in CPC and FPR, H₂O₂ added, and with and without MWTE spike. Experiments performed in the dark as control experiments (DC) are included as well.

Figure 6 shows As^{III} oxidation via solar HP; DC experiments apparently showed an increased oxidation, but most likely As^{III} adsorption onto TiO₂ surface is the main reason for this observation [69], as at pH = 8.5, As is mostly found as arsenious acid, which has a neutral charge [70]. The higher oxidation observed in HP experiments is clearly due to the generated ROS by HP, which also includes O₂^{•−} [71].

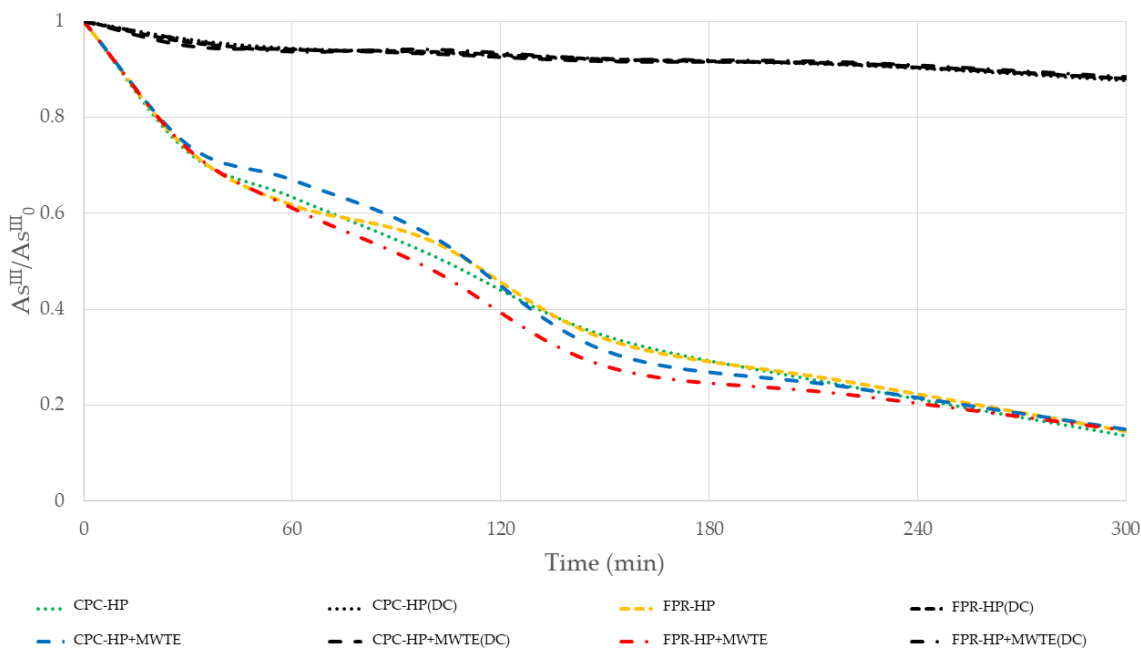


Figure 6. As^{III} heterogeneous photocatalytic (HP) oxidation experiments carried out both in CPC and FPR, and with and without MWTE spike. Experiments performed in the dark as control experiments (DC) are included as well.

In Figure 7, As^{III} oxidation via HP+ H₂O₂ is shown. The highest oxidation was achieved in this round of experiments, which conjoins the effects of the previous treatments. The main ROS driving As^{III} oxidation has been debated [72], but for cases in which H₂O₂ is added, it has been recently proposed that a nonradical species, surface complexes Ti-peroxo (Ti–OOH), would be the main oxidative species [73,74]. This fact can be theorized as an As^{III} oxidation experiment using cerium dioxide (CeO₂), with cerium being in the same periodic group as titanium, found in the presence of Ce-peroxo surface complexes [75]. Additionally, Ti–OOH (and Ce–OOH) has been reported as the main oxidative species in antimony (which is located in the same periodic group as As) oxidation experiments employing H₂O₂ over TiO₂/CeO₂ [76].

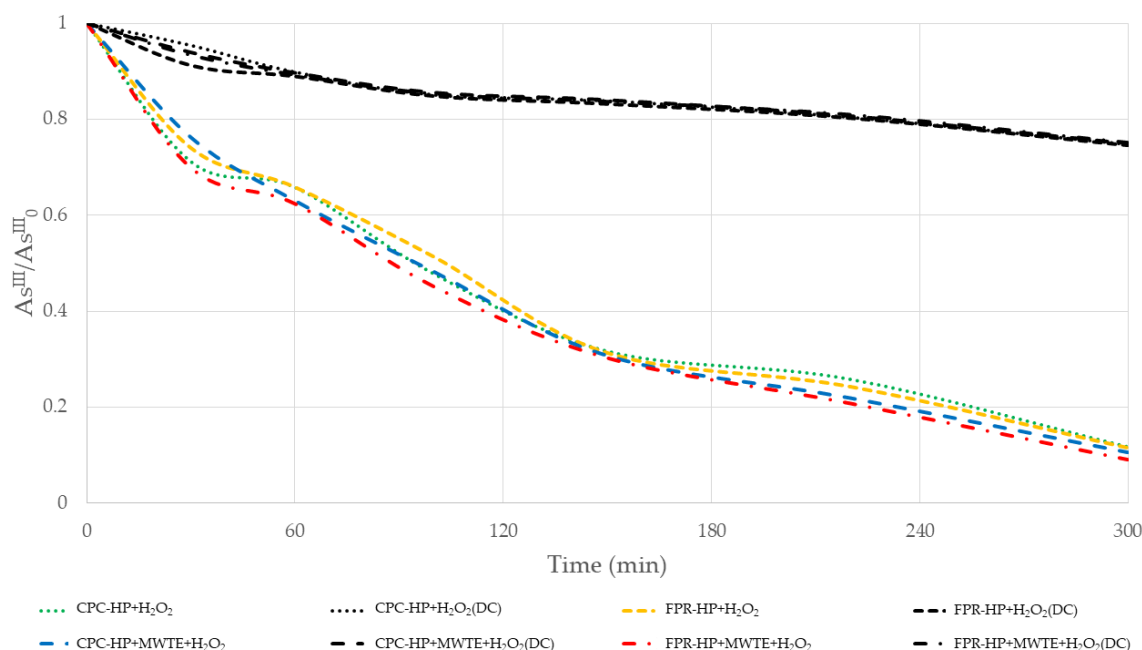


Figure 7. As^{III} heterogeneous photocatalytic (HP) oxidation experiments carried out both in CPC and FPR, H₂O₂ added, and with and without MWTE spike. Experiments performed in the dark as control experiments (DC) are included as well.

Since the groundwater matrix used in the experiments contained several cations and anions, other reactions could take place in some of the treatments; HO[•] can react with CO₃²⁻ and Cl⁻ to form carbonate and chloride radicals, respectively (CO₃^{•-} and Cl[•]); NO₃⁻ can give place to nitrite radical (NO₃[•]) [77]. Although the aim of this research is not to study the effect of said species in the outcome of As^{III} oxidation, it is worth mentioning that they may play a role in the whole process.

The pH did not remain constant throughout the experiments; however, the change was negligible (final pH > 8.0). Since As^{III} (in the form of arsenious acid) pK_a = 9.29 [78] and TiO₂ zero charge point is at pH = 6.3 [79], the pH change should not have a significant effect on the outcome of the experiment, not even after As^{III} oxidation, as the As^V pK_a values are pK_{a1} = 2.2, pK_{a2} = 7.08, and pK_{a3} = 11.5 [80].

3.2. Arsenic Removal

Water As concentration after chemical precipitation with FeCl₃ is reported in Table 4. Although more than 90% removal was achieved with every treatment, HP treatments were the only ones to attain an As concentration that complies with the WHO guidelines. Although it is well known that As^{III} is harder to remove than As^V due to its neutral charge [81,82], chemical precipitation is not a stoichiometric process and is also able to remove As [83]. The increased removal in DC samples involving H₂O₂ can be explained due to As^{III} oxidation caused by the Fenton reagent that is mostly carried out under

acidic conditions of $\text{pH} < 3$, but can also take place at higher pH values, at which point sedimentation will occur as well [84].

3.3. Coliform Disinfection

Total coliform disinfection results are presented in Table 5. DC experiments did not offer enough stress as to cause a noticeable effect in coliform MPN. Partial disinfection was observed when H_2O_2 was added, which can be attributed to both internal and external cell damage caused by the ROS [85]. Coliforms were not detected in solar experiments, which is expected as SODIS is a well-known point of use technology for water disinfection, which is effective for several microorganisms species [86]. It is inferred that disinfection could have happened faster in the treatments involving TiO_2 and H_2O_2 , as has been reported in a previous experiment [42].

As HP is nonselective, it can be used to deal with an assorted variety of contaminants [87] such as inactivating coliforms and oxidize arsenic as in the present case. This characteristic makes it attractive for further research and additional development to keep improving its technical feasibility. It is important to have options when it comes to water treatment and potabilization, as most of the times, one solution cannot fit to all cases.

3.4. Kinetic Analysis

The calculated rate constants, both photooxidative (k_{po}) and photocatalytic (K_{phC}), are shown in Table 6. The reaction rate constants for DC experiments were much lower than their irradiated counterparts in every case. H_2O_2 treatments also showed a higher reaction rate constant than those of treatments without H_2O_2 . The k_{po} values were lower than the K_{phC} values, and the higher reaction rate constants were observed in experimental runs with higher As^{III} oxidation. The coefficient of determination (R^2) for DC treatments was 0.87 on average, while for irradiated treatments it was 0.96, which is an acceptable value to fit the data to the pseudo first-order reaction model that has been reported to describe As^{III} heterogeneous photocatalytic oxidation [52,53].

3.5. Fluence Analysis

Table 7 presents the fluence and reaction rate constants as a function of Q_{UV} for each treatment. Fluence was lower in FPR treatments than in CPC treatments as the total irradiated surface is roughly 40% larger in the CPC than in the FPR. The proposed reaction rate constant in the function of Q_{UV} has been used to describe the kinetics of a reaction in function of cumulative UV dose as an alternative to kinetics in function of time [59]. The average R^2 value was 0.96, which is almost identical to the R^2 obtained when fitting the data to the pseudo first-order reaction model. It can be inferred that K_{UV} is suitable for explaining As^{III} oxidation via HP as well.

Table 4. Arsenic concentration after chemical precipitation with FeCl₃.

Treatment	As (µg/L)	As Removed (%)	Treatment	As (µg/L)	As Removed (%)
CPC-PO	23.4 ± 2.9	93.0 ± 0.9%	CPC-HP	8.9 ± 2.2	98.1 ± 0.6%
CPC-PO(DC)	25.1 ± 1.4	92.3 ± 0.4%	CPC-HP(DC)	22.7 ± 0.3	93.5 ± 0.1%
FPR-PO	20.72 ± 0.8	93.9 ± 0.3%	FPR-HP	8.2 ± 1.3	93.3 ± 0.4%
FPR-PO(DC)	24.3 ± 1.1	92.8 ± 0.3%	FPR-HP(DC)	16.2 ± 1.4	92.5 ± 1.1%
CPC-PO + MWTE	23.9 ± 0.8	93.3 ± 0.2%	CPC-HP + MWTE	9.2 ± 1.4	97.2 ± 0.4%
CPC-PO + MWTE(DC)	24.9 ± 2.1	92.5 ± 0.6%	CPC-HP + MWTE(DC)	21.1 ± 1.2	94 ± 0.4%
FPR-PO + MWTE	22.3 ± 2.5	92.8 ± 0.7%	FPR-HP + MWTE	8.3 ± 0.9	97.5 ± 0.3%
FPR-PO + MWTE(DC)	24.9 ± 2.1	92.6 ± 0.6%	FPR-HP + MWTE(DC)	23.3 ± 0.1	93.3 ± 0.1%
CPC-PO + H ₂ O ₂	16.5 ± 1.7	95.8 ± 0.5%	CPC-HP + H ₂ O ₂	5.3 ± 1.1	98.7 ± 0.3%
CPC-PO + H ₂ O ₂ (DC)	18.7 ± 0.5	94.5 ± 0.2%	CPC-HP + H ₂ O ₂ (DC)	10.2 ± 1.2	96.8 ± 0.4%
FPR-PO + H ₂ O ₂	16.5 ± 0.3	95.3 ± 0.1%	FPR-HP + H ₂ O ₂	5.1 ± 0.1	98.6 ± 0.0%
FPR-PO + H ₂ O ₂ (DC)	19.5 ± 0.7	94.2 ± 0.2%	FPR-HP + H ₂ O ₂ (DC)	10.2 ± 2.7	96.6 ± 0.8%
CPC-PO + MWTE + H ₂ O ₂	16.9 ± 0.8	94.9 ± 0.2%	CPC-HP + MWTE + H ₂ O ₂	1.6 ± 0.5	99.7 ± 0.1%
CPC-PO + MWTE + H ₂ O ₂ (DC)	18.7 ± 0.5	94.5 ± 0.2%	CPC-HP + MWTE + H ₂ O ₂ (DC)	11.8 ± 0.8	94.9 ± 0.2%
FPR-PO + MWTE + H ₂ O ₂	16.2 ± 0.2	95.5 ± 0.2%	FPR-HP + MWTE + H ₂ O ₂	1.7 ± 0.2	99.5 ± 0.1%
FPR-PO + MWTE + H ₂ O ₂ (DC)	18.7 ± 0.5	94.5 ± 0.2%	FPR-HP + MWTE + H ₂ O ₂ (DC)	11.5 ± 1.5	94.8 ± 0.4%

Table 5. Most probable number of coliforms in samples at the beginning and end of each treatment.

Treatment	0 min (MPN/100 mL)	300 min (MPN/100 mL)	Treatment	0 min (MPN/100 mL)	300 min (MPN/100 mL)
CPC-PO + MWTE	>2419	N.D. ^a	CPC-HP + MWTE	>2419	N.D.
CPC-PO + MWTE (DC)	>2419	>2419	CPC-HP + MWTE (DC)	>2419	>2419
FPR-PO + MWTE	>2419	N.D.	FPR-HP + MWTE	>2419	N.D.
FPR-PO + MWTE (DC)	>2419	>2419	FPR-HP + MWTE (DC)	>2419	>2419
CPC-PO + MWTE + H ₂ O ₂	>2419	N.D.	CPC-HP + MWTE + H ₂ O ₂	>2419	N.D.
CPC-PO + MWTE + H ₂ O ₂ (DC)	>2419	574–727	CPC-HP + MWTE + H ₂ O ₂ (DC)	>2419	658–755
FPR-PO + MWTE + H ₂ O ₂	>2419	N.D.	FPR-HP + MWTE + H ₂ O ₂	>2419	N.D.
FPR-PO + MWTE + H ₂ O ₂ (DC)	>2419	629–686	FPR-HP + MWTE + H ₂ O ₂ (DC)	>2419	613–689

Note: N.D.^a = Not detectable.**Table 6.** Calculated photooxidative and photocatalytic reaction rate constants for arsenic oxidation.

Treatment	k _{po} (×10 ⁻³ min ⁻¹)	Treatment	k _{po} (×10 ⁻³ min ⁻¹)	Treatment	K _{phC} (×10 ⁻³ min ⁻¹)	Treatment	K _{phC} (×10 ⁻³ min ⁻¹)
CPC-PO	0.8	CPC-PO + H ₂ O ₂	2.6	CPC-HP	6.2	CPC-HP + H ₂ O ₂	6.8
CPC-PO (DC)	0.2	CPC-PO + H ₂ O ₂ (DC)	0.8	CPC-HP (DC)	0.3	CPC-HP + H ₂ O ₂ (DC)	0.8
FPR-PO	0.8	FPR-PO + H ₂ O ₂	2.6	FPR-HP	6.0	FPR-HP + H ₂ O ₂	6.7
FPR-PO (DC)	0.2	FPR-PO + H ₂ O ₂ (DC)	0.8	FPR-HP (DC)	0.3	FPR-HP + H ₂ O ₂ (DC)	0.8

Table 7. Fluence and calculated reaction rate constants in function of fluence.

Treatment	Q_{UV} (kJ L ⁻¹)	K_{UV} ($\times 10^{-3}$ kJ ⁻¹ L)	Treatment	Q_{UV} (kJ L ⁻¹)	K_{UV} ($\times 10^{-3}$ kJ ⁻¹ L)
CPC-PO	354.99	0.7	FPR-PO	251.03	1.0
CPC-PO + H ₂ O ₂	339.45	2.2	FPR-PO + H ₂ O ₂	240.04	3.1
CPC-HP	366.79	5.1	FPR-HP	259.38	7.0
CPC-HP + H ₂ O ₂	361.57	5.6	FPR-HP + H ₂ O ₂	255.69	7.9

3.6. Collector Area per Order

Table 8 shows the A_{CO} value for each one of the treatments. A smaller A_{CO} is generally associated with a more efficient process [44]. On average, CPC needed 30% less photocatalyst covered area than the FPR, which is in accordance with the improved optical efficiency provided by the reflector [52], accounting for an improved use of the photocatalyst-covered area.

Table 8. Estimation of A_{CO} for each treatment and comparative efficiency between reactors, $\varepsilon = [(A_{CO_{FPR}} - A_{CO_{CPC}})/(A_{CO_{FPR}})] \times 100$, for arsenic oxidation, considering batch operation and a first-order rate reaction.

Treatment	A_{CO} (m ² ·m ⁻³ -Order)	Treatment	A_{CO} (m ² ·m ⁻³ -Order)	Efficiency (ε)
CPC-PO	83.3	FPR-PO	121.7	31.5
CPC-PO + H ₂ O ₂	28.4	FPR-PO + H ₂ O ₂	39.2	27.4
CPC-HP	11.3	FPR-HP	15.3	26.4
CPC-HP + H ₂ O ₂	10.2	FPR-HP + H ₂ O ₂	15.0	32.0

The A_{CO} for HP treatments was on average 75% more efficient than PO treatments ($\varepsilon = [(A_{CO_{PO}} - A_{CO_{HP}})/(A_{CO_{PO}})] \times 100$), while H₂O₂ treatments were 38% more efficient than treatments without H₂O₂ ($\varepsilon = [(A_{CO_{0mMH2O2}} - A_{CO_{1mMH2O2}})/(A_{CO_{0mMH2O2}})] \times 100$).

3.7. ANOVA Results

The summary of the ANOVA is shown in Table 9. The F-value for the model was statistically significant ($p < 0.05$); hence, it can be assumed that the linear model was appropriate for the analysis. The R^2 value was 0.76, leaving enough room for improvement for a better linear model that better explains variance [58].

Table 9. Summary of ANOVA for As^{III} oxidation.

Source	DF	Sum of Squares ($\times 10^4$)	Mean Square ($\times 10^4$)	F-Value	p -Value Probr > F
Model	6	4.7	0.7	49.61	<0.0001
AOP	1	1.3	1.3	88.53	<0.0001
H ₂ O ₂ addition	1	0.2	0.2	13.96	0.0003
MWTE spike	1	0.0	0.0	0.01	0.9355
Reactor employed	1	0.0	0.0	0.01	0.9410
Irradiation exposure	1	3.0	3.0	195.13	<0.0001
Q_{UV}	1	0.0	0.0	0.00	0.9662

The results obtained through the ANOVA support the observations made previously in Figures 4–7. The AOP effect was statistically significant; for PO, the UV light was the main driver for As^{III} oxidation, which is favored in alkaline conditions [88], but it is not as fast as HP, which promotes ROS generation to accelerate As^{III} oxidation [89]. H₂O₂ addition accelerated oxidation due to ROS generation [90] or Ti-peroxo species formation (in HP treatments only) [91]; hence, its effect being statically significant is within expectations.

Solar light exposure (whether or not as in DC treatments) was the most significant effect for As^{III} oxidation ($p < 0.05$ in all three cases).

The MWTE spike did not have a statistically significant effect on the As^{III} oxidation reaction rate, which is within the expectations of AOPs being nonselective [92]; it is evident that not every generated ROS is directed to As^{III}. The effect of the used reactor was not statistically significant either, despite the fact that their geometry allows for a completely different operation (light distribution, light propagation, surface area to volume ratio, etc. [93]). This finding supports the fact that the outcome of an HP operation might depend on a plethora of variables and the interactions between them, such as the photocatalyst properties, the source of light, the intensity of the light, the pH, the concentration of the pollutant, and the temperature of the geometry of the reactor [44]. Finally, the effect of the covariable, Q_{UV} , was not statistically significant, possibly because of uniformity in the timeframe of the operation, which translated into minimal Q_{UV} variations (solar noon operation and only on sunny days) [41,44] ($p < 0.05$ in all three cases).

3.8. Perspectives and Outlook

The present work results are in agreement with the HP TRL ongoing pilot scale applications. An As concentration of 300 $\mu\text{g/L}$ is extremely high, and the obtained results provide a notion of the resources needed to treat water with such characteristics. Disinfection can be achieved with solar light alone, but As^{III} oxidation was greatly improved when using HP, and even more with H₂O₂. Both TiO₂ and H₂O₂ pose no threat to the environment [94,95] and could be used readily. The present work analyzed only a volume of 3.5 L, and it took a considerable amount of time (300 min) to oxidize most of the As^{III}, so an optimization in function of time and volume treated with respect to As^{III} concentration should be followed, as proper experimental conditions have been found in the present work. Photocatalytic reactors are not easily scaled up due to the intrinsic nature of light; however, if space is available, scaling out is always possible [96].

TiO₂ is only active when irradiated with UV light, which limits its efficiency for solar applications, as UV light accounts for less than 5% of the received solar energy [97]; a direct comparison against visible light-active photocatalysts should also be explored. TiO₂ exhibits visible light activity when doped with some elements, for example nitrogen or silver [98].

4. Conclusions

The treatments CPC-HP + H₂O₂ and FPR-HP + H₂O₂ yielded the best oxidation for As^{III}, with rates around 90%. These treatments also exhibited the highest oxidation reaction rate constants, with $6.8 \times 10^{-3} \text{ min}^{-1}$ and $6.7 \times 10^{-3} \text{ min}^{-1}$, respectively.

As removal rates achieved via chemical precipitation for the aforementioned treatments were 98.7% and 98.6%, reaching the As concentration level recommended by the WHO, which is below 10 $\mu\text{g/L}$.

Additionally, no coliforms were detected in the irradiated treatments, which adds up to the advantages of HP as a potential and promising technology for water potabilization and wastewater treatment.

The determination of A_{CO} showed that CPC was on average 30% more efficient than the FPR, requiring less photocatalyst-covered area.

The effects of AOP, H₂O₂ addition, and light irradiation were statistically significant for the As^{III} oxidation reaction rate, while the type of reactor utilized, spiking with MWTE, or fluence were not ($p < 0.05$), as found out with an ANOVA.

Supplementary Materials: The following supporting information can be downloaded at: <https://www.mdpi.com/article/10.3390/w14152450/s1>, Table S1: FeCl₃ dose and As concentration in the supernatant. References [47,99–101] are cited in the supplementary materials.

Author Contributions: Conceptualization, F.d.J.S.-V. and J.B.P.-N.; Data curation, F.d.J.S.-V.; Formal analysis, F.d.J.S.-V. and C.M.N.-N.; Investigation, F.d.J.S.-V.; Methodology, F.d.J.S.-V. and J.B.P.-N.; Resources, J.B.P.-N. and M.T.A.-H.; Supervision, J.B.P.-N. and M.T.A.-H.; Visualization, C.M.N.-N., J.B.P.-N. and M.T.A.-H.; Writing—original draft, F.d.J.S.-V.; Writing—review and editing, C.M.N.-N., J.B.P.-N. and M.T.A.-H. All authors have read and agreed to the published version of the manuscript.

Funding: The research was internally financed by Centro de Investigación en Materiales Avanzados and Instituto Politécnico Nacional (SIP project: 20210507). The first author is grateful to the Consejo Nacional de Ciencia y Tecnología (CONACyT) through the doctorate scholarship granted to him, student identification DCTA1001002.

Institutional Review Board Statement: Not applicable.

Informed Consent Statement: Not applicable.

Data Availability Statement: All data and materials have been provided within the manuscript.

Acknowledgments: The authors would like to thank academic technicians Luis Arturo Torres Castañón and José Rafael Irigoyen Campuzano for their valuable collaboration in the analytical determinations.

Conflicts of Interest: The authors declare no conflict of interest to disclose. Funders played no role in study design; data collection, analysis, and interpretation; manuscript writing, and results publication.

References

1. Mandal, B. Arsenic Round the World: A Review. *Talanta* **2002**, *58*, 201–235. [[CrossRef](#)]
2. Urseler, N.; Bachetti, R.; Morgante, V.; Agostini, E.; Morgante, C. Groundwater Quality and Vulnerability in Farms from Agricultural-Dairy Basin of the Argentine Pampas. *Environ. Sci. Pollut. Res.* **2022**. [[CrossRef](#)]
3. Jain, N.; Chandramani, S. Arsenic Poisoning- An Overview. *Indian J. Med. Spec.* **2018**, *9*, 143–145. [[CrossRef](#)]
4. Flora, S.J.S. Arsenic and Dichlorvos: Possible Interaction between Two Environmental Contaminants. *J. Trace Elem. Med. Biol.* **2016**, *35*, 43–60. [[CrossRef](#)]
5. Bjørklund, G.; Oliinyk, P.; Lysiuk, R.; Rahaman, M.S.; Antonyak, H.; Lozynska, I.; Lenchyk, L.; Peana, M. Arsenic Intoxication: General Aspects and Chelating Agents. *Arch. Toxicol.* **2020**, *94*, 1879–1897. [[CrossRef](#)]
6. Anand, V.; Kaur, J.; Srivastava, S.; Bist, V.; Singh, P.; Srivastava, S. Arsenotrophy: A Pragmatic Approach for Arsenic Bioremediation. *J. Environ. Chem. Eng.* **2022**, *10*, 107528. [[CrossRef](#)]
7. Yu, S.; Li, L.-H.; Lee, C.-H.; Jeyakannu, P.; Wang, J.-J.; Hong, C.-H. Arsenic Leads to Autophagy of Keratinocytes by Increasing Aquaporin 3 Expression. *Sci. Rep.* **2021**, *11*, 17523. [[CrossRef](#)]
8. García-Rosales, G.; Longoria-Gándara, L.C.; Cruz-Cruz, G.J.; Olayo-González, M.G.; Mejía-Cuero, R.; Pérez, P.Á. Fe-TiO_x Nanoparticles on Pineapple Peel: Synthesis, Characterization and As(V) Sorption. *Environ. Nanotechnol. Monit. Manag.* **2018**, *9*, 112–121. [[CrossRef](#)]
9. Khan, M.I.; Ahmad, M.F.; Ahmad, I.; Ashfaq, F.; Wahab, S.; Alsayegh, A.A.; Kumar, S.; Hakeem, K.R. Arsenic Exposure through Dietary Intake and Associated Health Hazards in the Middle East. *Nutrients* **2022**, *14*, 2136. [[CrossRef](#)]
10. Guglielmi, G. Arsenic in Drinking Water Threatens up to 60 Million in Pakistan. *Science* **2017**, *14*, 2136. [[CrossRef](#)]
11. World Health Organization. *Guidelines for Drinking-Water Quality: Fourth Edition Incorporating the First Addendum*; World Health Organization: Geneva, Switzerland, 2017.
12. Fatoki, J.O.; Badmus, J.A. Arsenic as an Environmental and Human Health Antagonist: A Review of Its Toxicity and Disease Initiation. *J. Hazard. Mater. Adv.* **2022**, *5*, 100052. [[CrossRef](#)]
13. Raju, N.J. Arsenic in the Geo-Environment: A Review of Sources, Geochemical Processes, Toxicity and Removal Technologies. *Environ. Res.* **2022**, *203*, 111782. [[CrossRef](#)]
14. Taviani, E.; Pedro, O. Impact of the Aquatic Pathobiome in Low-Income and Middle-Income Countries (LMICs) Quest for Safe Water and Sanitation Practices. *Curr. Opin. Biotechnol.* **2022**, *73*, 220–224. [[CrossRef](#)]
15. Hanif, Z.; Tariq, M.Z.; Khan, Z.A.; La, M.; Choi, D.; Park, S.J. Polypyrrole-Coated Nanocellulose for Solar Steam Generation: A Multi-Surface Photothermal Ink with Antibacterial and Antifouling Properties. *Carbohydr. Polym.* **2022**, *292*, 119701. [[CrossRef](#)]
16. Javaid, M.; Qasim, H.; Zia, H.Z.; Bashir, M.A.; Syeda Amber Hameed, A.Q.; Samiullah, K.; Hashem, M.; Morsy, K.; Dajem, S.B.; Muhammad, T.; et al. Bacteriological Composition of Groundwater and Its Role in Human Health. *J. King Saud Univ. Sci.* **2022**, *34*, 102128. [[CrossRef](#)]
17. Adelodun, B.; Ajibade, F.O.; Ighalo, J.O.; Odey, G.; Ibrahim, R.G.; Kareem, K.Y.; Bakare, H.O.; Tihamiyu, A.O.; Ajibade, T.F.; Abdulkadir, T.S.; et al. Assessment of Socioeconomic Inequality Based on Virus-Contaminated Water Usage in Developing Countries: A Review. *Environ. Res.* **2021**, *192*, 110309. [[CrossRef](#)]
18. Ahmad, A.; Bhattacharya, P. Arsenic in Drinking Water: Is 10 Mg/L a Safe Limit? *Curr. Pollut. Rep.* **2019**, *5*, 1–3. [[CrossRef](#)]
19. Wen, X.; Chen, F.; Lin, Y.; Zhu, H.; Yuan, F.; Kuang, D.; Jia, Z.; Yuan, Z. Microbial Indicators and Their Use for Monitoring Drinking Water Quality—A Review. *Sustainability* **2020**, *12*, 2249. [[CrossRef](#)]

20. Valdiviezo Gonzales, L.G.; García Ávila, F.F.; Cabello Torres, R.J.; Castañeda Olivera, C.A.; Alfaro Paredes, E.A. Scientometric Study of Drinking Water Treatments Technologies: Present and Future Challenges. *Cogent Eng.* **2021**, *8*, 1929046. [[CrossRef](#)]
21. Sundar, K.P.; Kanmani, S. Progression of Photocatalytic Reactors and It's Comparison: A Review. *Chem. Eng. Res. Des.* **2020**, *154*, 135–150. [[CrossRef](#)]
22. Jabbar, Z.H.; Esmail Ebrahim, S. Recent Advances in Nano-Semiconductors Photocatalysis for Degrading Organic Contaminants and Microbial Disinfection in Wastewater: A Comprehensive Review. *Environ. Nanotechnol. Monit. Manag.* **2022**, *17*, 100666. [[CrossRef](#)]
23. Sibhatu, A.K.; Weldegebrieal, G.K.; Sagadevan, S.; Tran, N.N.; Hessel, V. Photocatalytic Activity of CuO Nanoparticles for Organic and Inorganic Pollutants Removal in Wastewater Remediation. *Chemosphere* **2022**, *300*, 134623. [[CrossRef](#)]
24. Wang, H.; Li, X.; Zhao, X.; Li, C.; Song, X.; Zhang, P.; Huo, P.; Li, X. A Review on Heterogeneous Photocatalysis for Environmental Remediation: From Semiconductors to Modification Strategies. *Chin. J. Catal.* **2022**, *43*, 178–214. [[CrossRef](#)]
25. Xie, L.; Hao, J.G.; Chen, H.Q.; Li, Z.X.; Ge, S.Y.; Mi, Y.; Yang, K.; Lu, K.Q. Recent Advances of Nickel Hydroxide-Based Cocatalysts in Heterogeneous Photocatalysis. *Catal. Commun.* **2022**, *162*, 106371. [[CrossRef](#)]
26. Karim, A.V.; Krishnan, S.; Shriwastav, A. An Overview of Heterogeneous Photocatalysis for the Degradation of Organic Compounds: A Special Emphasis on Photocorrosion and Reusability. *J. Indian Chem. Soc.* **2022**, *99*, 100480. [[CrossRef](#)]
27. Sharma, A.; Ahmad, J.; Flora, S.J.S. Application of Advanced Oxidation Processes and Toxicity Assessment of Transformation Products. *Environ. Res.* **2018**, *167*, 223–233. [[CrossRef](#)]
28. Marinho, B.A.; Cristóvão, R.O.; Boaventura, R.A.R.; Vilar, V.J.P. As(III) and Cr(VI) Oxyanion Removal from Water by Advanced Oxidation/Reduction Processes—A Review. *Environ. Sci. Pollut. Res.* **2019**, *26*, 2203–2227. [[CrossRef](#)]
29. García, F.E.; Litter, M.I.; Sora, I.N. Assessment of the Arsenic Removal From Water Using Lanthanum Ferrite. *ChemistryOpen* **2021**, *10*, 790–797. [[CrossRef](#)]
30. Deng, Y.; Li, Y.; Li, X.; Sun, Y.; Ma, J.; Lei, M.; Weng, L. Influence of Calcium and Phosphate on PH Dependency of Arsenite and Arsenate Adsorption to Goethite. *Chemosphere* **2018**, *199*, 617–624. [[CrossRef](#)]
31. Hosseini, F.; Assadi, A.A.; Nguzen-Tri, P.; Ali, I.; Rtimi, S. Titanium-Based Photocatalytic Coatings for Bacterial Disinfection: The Shift from Suspended Powders to Catalytic Interfaces. *Surf. Interfaces* **2022**, *32*, 102078. [[CrossRef](#)]
32. John, D.; Jose, J.; Bhat, S.G.; Achari, V.S. Integration of Heterogeneous Photocatalysis and Persulfate Based Oxidation Using TiO₂-Reduced Graphene Oxide for Water Decontamination and Disinfection. *Heliyon* **2021**, *7*, e07451. [[CrossRef](#)] [[PubMed](#)]
33. Byrne, J.; Dunlop, P.; Hamilton, J.; Fernández-Ibáñez, P.; Polo-López, I.; Sharma, P.; Vennard, A. A Review of Heterogeneous Photocatalysis for Water and Surface Disinfection. *Molecules* **2015**, *20*, 5574–5615. [[CrossRef](#)] [[PubMed](#)]
34. Xu, Y.; Liu, Q.; Liu, C.; Zhai, Y.; Xie, M.; Huang, L.; Xu, H.; Li, H.; Jing, J. Visible-Light-Driven Ag/AgBr/ZnFe₂O₄ Composites with Excellent Photocatalytic Activity for *E. coli* Disinfection and Organic Pollutant Degradation. *J. Colloid Interface Sci.* **2018**, *512*, 555–566. [[CrossRef](#)] [[PubMed](#)]
35. Serrà, A.; Philippe, L.; Perreault, F.; Garcia-Segura, S. Photocatalytic Treatment of Natural Waters. Reality or Hype? The Case of Cyanotoxins Remediation. *Water Res.* **2021**, *188*, 116543. [[CrossRef](#)] [[PubMed](#)]
36. Antonopoulou, M.; Kosma, C.; Albanis, T.; Konstantinou, I. An Overview of Homogeneous and Heterogeneous Photocatalysis Applications for the Removal of Pharmaceutical Compounds from Real or Synthetic Hospital Wastewaters under Lab or Pilot Scale. *Sci. Total Environ.* **2021**, *765*, 144163. [[CrossRef](#)]
37. Espíndola, J.C.; Vilar, V.J.P. Innovative Light-Driven Chemical/Catalytic Reactors towards Contaminants of Emerging Concern Mitigation: A Review. *Chem. Eng. J.* **2020**, *394*, 124865. [[CrossRef](#)]
38. Chen, L.; Tang, J.; Song, L.-N.; Chen, P.; He, J.; Au, C.-T.; Yin, S.-F. Heterogeneous Photocatalysis for Selective Oxidation of Alcohols and Hydrocarbons. *Appl. Catal. B Environ.* **2019**, *242*, 379–388. [[CrossRef](#)]
39. Binjhade, R.; Mondal, R.; Mondal, S. Continuous Photocatalytic Reactor: Critical Review on the Design and Performance. *J. Environ. Chem. Eng.* **2022**, *10*, 107746. [[CrossRef](#)]
40. Zaruma-Arias, P.E.; Núñez-Núñez, C.M.; González-Burciaga, L.A.; Proal-Nájera, J.B. Solar Heterogeneous Photocatalytic Degradation of Methylthionine Chloride on a Flat Plate Reactor: Effect of PH and H₂O₂ Addition. *Catalysts* **2022**, *12*, 132. [[CrossRef](#)]
41. Silerio-Vázquez, F.; Alarcón-Herrera, M.T.; Proal-Nájera, J.B. Solar Heterogeneous Photocatalytic Degradation of Phenol on TiO₂/Quartz and TiO₂/Calcite: A Statistical and Kinetic Approach on Comparative Efficiencies towards a TiO₂/Glass System. *Environ. Sci. Pollut. Res.* **2022**, *29*, 42319–42330. [[CrossRef](#)]
42. Núñez-Núñez, C.M.; Osorio-Revilla, G.I.; Villanueva-Fierro, I.; Antileo, C.; Proal-Nájera, J.B. Solar Fecal Coliform Disinfection in a Wastewater Treatment Plant by Oxidation Processes: Kinetic Analysis as a Function of Solar Radiation. *Water* **2020**, *12*, 639. [[CrossRef](#)]
43. González-Burciaga, L.A.; Núñez-Núñez, C.M.; Morones-Esquivel, M.M.; Avila-Santos, M.; Lemus-Santana, A.; Proal-Nájera, J.B. Characterization and Comparative Performance of TiO₂ Photocatalysts on 6-Mercaptopurine Degradation by Solar Heterogeneous Photocatalysis. *Catalysts* **2020**, *10*, 118. [[CrossRef](#)]
44. Silerio-Vázquez, F.d.J.; Núñez-Núñez, C.M.; Alarcón-Herrera, M.T.; Proal-Nájera, J.B. Comparative Efficiencies for Phenol Degradation on Solar Heterogeneous Photocatalytic Reactors: Flat Plate and Compound Parabolic Collector. *Catalysts* **2022**, *12*, 575. [[CrossRef](#)]

45. Leiva-Aravena, E.; Vera, M.A.; Nerenberg, R.; Leiva, E.D.; Vargas, I.T. Biofilm Formation of *Ancylobacter* Sp. TS-1 on Different Granular Materials and Its Ability for Chemolithoautotrophic As(III)-Oxidation at High Concentrations. *J. Hazard. Mater.* **2022**, *421*, 126733. [[CrossRef](#)] [[PubMed](#)]
46. Vieira, B.R.C.; Pintor, A.M.A.; Boaventura, R.A.R.; Botelho, C.M.S.; Santos, S.C.R. Arsenic Removal from Water Using Iron-Coated Seaweeds. *J. Environ. Manag.* **2017**, *192*, 224–233. [[CrossRef](#)] [[PubMed](#)]
47. Laky, D.; Licskó, I. Arsenic Removal by Ferric-Chloride Coagulation—Effect of Phosphate, Bicarbonate and Silicate. *Water Sci. Technol.* **2011**, *64*, 1046–1055. [[CrossRef](#)]
48. Cravo, A.; Barbosa, A.B.; Correia, C.; Matos, A.; Caetano, S.; Lima, M.J.; Jacob, J. Unravelling the Effects of Treated Wastewater Discharges on the Water Quality in a Coastal Lagoon System (Ria Formosa, South Portugal): Relevance of Hydrodynamic Conditions. *Mar. Pollut. Bull.* **2022**, *174*, 113296. [[CrossRef](#)]
49. Luvhimbi, N.; Tshitangano, T.G.; Mabunda, J.T.; Olaniyi, F.C.; Edokpayi, J.N. Water Quality Assessment and Evaluation of Human Health Risk of Drinking Water from Source to Point of Use at Thulamela Municipality, Limpopo Province. *Sci. Rep.* **2022**, *12*, 6059. [[CrossRef](#)]
50. Hile, T.D.; Dunbar, S.G.; Sinclair, R.G. Microbial Contamination of Drinking Water from Vending Machines of Eastern Coachella Valley. *Water Supply* **2021**, *21*, 1618–1628. [[CrossRef](#)]
51. Horváth, E.; Gabathuler, J.; Bourdieu, G.; Vidal-Revel, E.; Benthem Muñoz, M.; Gaal, M.; Grandjean, D.; Breider, F.; Rossi, L.; Sienkiewicz, A.; et al. Solar Water Purification with Photocatalytic Nanocomposite Filter Based on TiO₂ Nanowires and Carbon Nanotubes. *npj Clean Water* **2022**, *5*, 10. [[CrossRef](#)]
52. García, A.; Rosales, M.; Thomas, M.; Golemme, G. Arsenic Photocatalytic Oxidation over TiO₂-Loaded SBA-15. *J. Environ. Chem. Eng.* **2021**, *9*, 106443. [[CrossRef](#)]
53. Wei, Z.; Fang, Y.; Wang, Z.; Liu, Y.; Wu, Y.; Liang, K.; Yan, J.; Pan, Z.; Hu, G. PH Effects of the Arsenite Photocatalytic Oxidation Reaction on Different Anatase TiO₂ Facets. *Chemosphere* **2019**, *225*, 434–442. [[CrossRef](#)] [[PubMed](#)]
54. Kanth, N.; Xu, W.; Prasad, U.; Ravichandran, D.; Kannan, A.M.; Song, K. PMMA-TiO₂ Fibers for the Photocatalytic Degradation of Water Pollutants. *Nanomaterials* **2020**, *10*, 1279. [[CrossRef](#)] [[PubMed](#)]
55. Li, Z.; Zhang, Z.; Dong, Z.; Wu, Y.; Zhu, X.; Cheng, Z.; Liu, Y.; Wang, Y.; Zheng, Z.; Cao, X.; et al. CuS/TiO₂ Nanotube Arrays Heterojunction for the Photoreduction of Uranium (VI). *J. Solid State Chem.* **2021**, *303*, 122499. [[CrossRef](#)]
56. Kuhn, H.; Försterling, H.-D.; Waldeck, D.H. Chemical Kinetics. In *Principles of Physical Chemistry*; John Wiley & Sons, LTD: West Sussex, UK, 2000; pp. 735–794, ISBN 978-0-470-08964-4.
57. Giménez, J.; Curcó, D.; Queral, M. Photocatalytic Treatment of Phenol and 2,4-Dichlorophenol in a Solar Plant in the Way to Scaling-Up. *Catal. Today* **1999**, *54*, 229–243. [[CrossRef](#)]
58. Gutiérrez-Alfaro, S.; Acevedo, A.; Rodríguez, J.; Carpio, E.A.; Manzano, M.A. Solar Photocatalytic Water Disinfection of *Escherichia coli*, *Enterococcus* spp. and *Clostridium perfringens* Using Different Low-Cost Devices. *J. Chem. Technol. Biotechnol.* **2016**, *91*, 2026–2037. [[CrossRef](#)]
59. Mac Mahon, J.; Pillai, S.C.; Kelly, J.M.; Gill, L.W. Solar Photocatalytic Disinfection of *E. Coli* and Bacteriophages MS2, ΦX174 and PR772 Using TiO₂, ZnO and Ruthenium Based Complexes in a Continuous Flow System. *J. Photochem. Photobiol. B Biol.* **2017**, *170*, 79–90. [[CrossRef](#)]
60. Pereira, J.H.O.S.; Vilar, V.J.P.; Borges, M.T.; González, O.; Esplugas, S.; Boaventura, R.A.R. Photocatalytic Degradation of Oxytetracycline Using TiO₂ under Natural and Simulated Solar Radiation. *Sol. Energy* **2011**, *85*, 2732–2740. [[CrossRef](#)]
61. Rincón, A.-G.; Pulgarin, C. Field Solar *E. Coli* Inactivation in the Absence and Presence of TiO₂: Is UV Solar Dose an Appropriate Parameter for Standardization of Water Solar Disinfection? *Sol. Energy* **2004**, *77*, 635–648. [[CrossRef](#)]
62. Bolton, J.R.; Bircher, K.G.; Tumas, W.; Tolman, C.A. Figures-of-Merit for the Technical Development and Application of Advanced Oxidation Technologies for Both Electric- and Solar-Driven Systems (IUPAC Technical Report). *Pure Appl. Chem.* **2001**, *73*, 627–637. [[CrossRef](#)]
63. Faul, F.; Erdfelder, E.; Buchner, A.; Lang, A.-G. Statistical Power Analyses Using G*Power 3.1: Tests for Correlation and Regression Analyses. *Behav. Res. Methods* **2009**, *41*, 1149–1160. [[CrossRef](#)]
64. Manjiao, C.; Zhengfu, Z.; Xinjun, H.; Jianping, T.; Jingsong, W.; Rundong, W.; Xian, Z.; Xinjun, Z.; PeiLun, S.; Dianwen, L. Oxidation Mechanism of the Arsenopyrite Surface by Oxygen with and without Water: Experimental and Theoretical Analysis. *Appl. Surf. Sci.* **2022**, *573*, 151574. [[CrossRef](#)]
65. Heiba, H.F.; Bullen, J.C.; Kafizas, A.; Petit, C.; Skinner, S.J.; Weiss, D. The Determination of Oxidation Rates and Quantum Yields during the Photocatalytic Oxidation of As(III) over TiO₂. *J. Photochem. Photobiol. A Chem.* **2022**, *424*, 113628. [[CrossRef](#)]
66. Su, J.; Lyu, T.; Cooper, M.; Mortimer, R.J.G.; Pan, G. Efficient Arsenic Removal by a Bifunctional Heterogeneous Catalyst through Simultaneous Hydrogen Peroxide (H₂O₂) Catalytic Oxidation and Adsorption. *J. Clean. Prod.* **2021**, *325*, 129329. [[CrossRef](#)]
67. Wang, X.; Chen, J.; Bu, Z.; Wang, H.; Wang, W.; Li, W.; Sun, T. Accelerated C-Face Polishing of Silicon Carbide by Alkaline Polishing Slurries with Fe₃O₄ Catalysts. *J. Environ. Chem. Eng.* **2021**, *9*, 106863. [[CrossRef](#)]
68. Hong, J.; Liu, L.; Ning, Z.; Liu, C.; Qiu, G. Synergistic Oxidation of Dissolved As(III) and Arsenopyrite in the Presence of Oxygen: Formation and Function of Reactive Oxygen Species. *Water Res.* **2021**, *202*, 117416. [[CrossRef](#)]
69. Song, J.; Yan, L.; Duan, J.; Jing, C. TiO₂ Crystal Facet-Dependent Antimony Adsorption and Photocatalytic Oxidation. *J. Colloid Interface Sci.* **2017**, *496*, 522–530. [[CrossRef](#)]
70. Ning, R.Y. Arsenic Removal by Reverse Osmosis. *Desalination* **2002**, *143*, 237–241. [[CrossRef](#)]

71. Litter, M.I. Last Advances on TiO₂-Photocatalytic Removal of Chromium, Uranium and Arsenic. *Curr. Opin. Green Sustain. Chem.* **2017**, *6*, 150–158. [[CrossRef](#)]
72. Silerio-Vázquez, F.; Proal Nájera, J.B.; Bundschuh, J.; Alarcon-Herrera, M.T. Photocatalysis for Arsenic Removal from Water: Considerations for Solar Photocatalytic Reactors. *Environ. Sci. Pollut. Res.* **2021**. [[CrossRef](#)]
73. Meng, F.; Zhang, S.; Zeng, Y.; Zhang, M.; Zou, H.; Zhong, Q.; Li, Y. Promotional Effect of Surface Fluorine on TiO₂: Catalytic Conversion of O₃ and H₂O₂ into ·OH and ·O₂⁻ Radicals for High-Efficiency NO Oxidation. *Chem. Eng. J.* **2021**, *424*, 130358. [[CrossRef](#)]
74. Naniwa, S.; Yamamoto, A.; Yoshida, H. Visible Light-Induced Minisci Reaction through Photoexcitation of Surface Ti-Peroxo Species. *Catal. Sci. Technol.* **2021**, *11*, 3376–3384. [[CrossRef](#)]
75. Shan, C.; Liu, Y.; Huang, Y.; Pan, B. Non-Radical Pathway Dominated Catalytic Oxidation of As(III) with Stoichiometric H₂O₂ over Nanoceria. *Environ. Int.* **2019**, *124*, 393–399. [[CrossRef](#)] [[PubMed](#)]
76. Ren, Y.; Liu, Y.; Liu, F.; Li, F.; Shen, C.; Wu, Z. Extremely Efficient Electro-Fenton-like Sb(III) Detoxification Using Nanoscale Ti-Ce Binary Oxide: An Effective Design to Boost Catalytic Activity via Non-Radical Pathway. *Chin. Chem. Lett.* **2021**, *32*, 2519–2523. [[CrossRef](#)]
77. Ghanbari, F.; Giannakis, S.; Lin, K.-Y.A.; Wu, J.; Madihi-Bidgoli, S. Acetaminophen Degradation by a Synergistic Peracetic Acid/UVC-LED/Fe(II) Advanced Oxidation Process: Kinetic Assessment, Process Feasibility and Mechanistic Considerations. *Chemosphere* **2021**, *263*, 128119. [[CrossRef](#)]
78. Zhang, X.; Dong, Q.; Wang, Y.; Zhu, Z.; Guo, Z.; Li, J.; Lv, Y.; Chow, Y.T.; Wang, X.; Zhu, L.; et al. Water-Stable Metal–Organic Framework (UiO-66) Supported on Zirconia Nanofibers Membrane for the Dynamic Removal of Tetracycline and Arsenic from Water. *Appl. Surf. Sci.* **2022**, *596*, 153559. [[CrossRef](#)]
79. Lou, T.; Song, S.; Gao, X.; Qian, W.; Chen, X.; Li, Q. Sub-20-Nm Anatase TiO₂ Anchored on Hollow Carbon Spheres for Enhanced Photocatalytic Degradation of Reactive Red 195. *J. Colloid Interface Sci.* **2022**, *617*, 663–672. [[CrossRef](#)]
80. Dudek, S.; Kołodziejka, D. Arsenic(V) Removal on the Lanthanum-Modified Ion Exchanger with Quaternary Ammonium Groups Based on Iron Oxide. *J. Mol. Liq.* **2022**, *347*, 117985. [[CrossRef](#)]
81. Chi, Z.; Zhu, Y.; Liu, W.; Huang, H.; Li, H. Selective Removal of As(III) Using Magnetic Graphene Oxide Ion-Imprinted Polymer in Porous Media: Potential Effect of External Magnetic Field. *J. Environ. Chem. Eng.* **2021**, *9*, 105671. [[CrossRef](#)]
82. Zeng, H.; Zhai, L.; Qiao, T.; Yu, Y.; Zhang, J.; Li, D. Efficient Removal of As(V) from Aqueous Media by Magnetic Nanoparticles Prepared with Iron-Containing Water Treatment Residuals. *Sci. Rep.* **2020**, *10*, 9335. [[CrossRef](#)]
83. Weerasundara, L.; Ok, Y.-S.; Bundschuh, J. Selective Removal of Arsenic in Water: A Critical Review. *Environ. Pollut.* **2021**, *268*, 115668. [[CrossRef](#)]
84. Hug, S.J.; Leupin, O. Iron-Catalyzed Oxidation of Arsenic (III) by Oxygen and by Hydrogen Peroxide: pH-Dependent Formation of Oxidants in the Fenton Reaction. *Environ. Sci. Technol.* **2003**, *37*, 2734–2742. [[CrossRef](#)]
85. García-Gil, Á.; Feng, L.; Moreno-SanSegundo, J.; Giannakis, S.; Pulgarín, C.; Marugán, J. Mechanistic Modelling of Solar Disinfection (SODIS) Kinetics of *Escherichia coli*, Enhanced with H₂O₂—Part 2: Shine on You, Crazy Peroxide. *Chem. Eng. J.* **2022**, *439*, 135783. [[CrossRef](#)]
86. Cowie, B.E.; Porley, V.; Robertson, N. Solar Disinfection (SODIS) Provides a Much Underexploited Opportunity for Researchers in Photocatalytic Water Treatment (PWT). *ACS Catal.* **2020**, *10*, 11779–11782. [[CrossRef](#)]
87. Oturan, M.A.; Aaron, J.-J.J. Advanced Oxidation Processes in Water/Wastewater Treatment: Principles and Applications. A Review. *Crit. Rev. Environ. Sci. Technol.* **2014**, *44*, 2577–2641. [[CrossRef](#)]
88. Amyot, M.; Bélanger, D.; Simon, D.F.; Chételat, J.; Palmer, M.; Ariya, P. Photooxidation of Arsenic in Pristine and Mine-Impacted Canadian Subarctic Freshwater Systems. *J. Hazard. Mater. Adv.* **2021**, *2*, 100006. [[CrossRef](#)]
89. Saleh, S.; Mohammadnejad, S.; Khorgooei, H.; Otadi, M. Photooxidation/Adsorption of Arsenic (III) in Aqueous Solution over Bentonite/Chitosan/TiO₂ Heterostructured Catalyst. *Chemosphere* **2021**, *280*, 130583. [[CrossRef](#)]
90. Shen, J.; Yu, H.; Shu, Y.; Ma, M.; Chen, H. A Robust ROS Generation Strategy for Enhanced Chemodynamic/Photodynamic Therapy via H₂O₂/O₂ Self-Supply and Ca²⁺ Overloading. *Adv. Funct. Mater.* **2021**, *31*, 2106106. [[CrossRef](#)]
91. Huang, L.; Liu, S.; Li, X.; Peng, X.; Liu, D. Controllable High-Efficiency Transformation of H₂O₂ to Reactive Oxygen Species via Electroactivation of Ti-Peroxo Complexes. *Sep. Purif. Technol.* **2022**, *289*, 120747. [[CrossRef](#)]
92. Pretali, L.; Fasani, E.; Sturini, M. Current Advances on the Photocatalytic Degradation of Fluoroquinolones: Photoreaction Mechanism and Environmental Application. *Photochem. Photobiol. Sci.* **2022**, *21*, 899–912. [[CrossRef](#)]
93. Abdel-Maksoud, Y.K.; Imam, E.; Ramadan, A.R. TiO₂ Water-Bell Photoreactor for Wastewater Treatment. *Sol. Energy* **2018**, *170*, 323–335. [[CrossRef](#)]
94. Ding, Y.; Zhou, W.; Gao, J.; Sun, F.; Zhao, G. H₂O₂ Electrogeneration from O₂ Electroreduction by N-Doped Carbon Materials: A Mini-Review on Preparation Methods, Selectivity of N Sites, and Prospects. *Adv. Mater. Interfaces* **2021**, *8*, 2002091. [[CrossRef](#)]
95. Dharma, H.N.C.; Jaafar, J.; Widiastuti, N.; Matsuyama, H.; Rajabsadeh, S.; Othman, M.H.D.; Rahman, M.A.; Jafri, N.N.M.; Suhaimin, N.S.; Nasir, A.M.; et al. A Review of Titanium Dioxide (TiO₂)-Based Photocatalyst for Oilfield-Produced Water Treatment. *Membranes* **2022**, *12*, 345. [[CrossRef](#)] [[PubMed](#)]

96. Zhang, J.; Mo, Y. A Scalable Light-Diffusing Photochemical Reactor for Continuous Processing of Photoredox Reactions. *Chem. Eng. J.* **2022**, *435*, 134889. [[CrossRef](#)]
97. Kanakaraju, D.; anak Kutiang, F.D.; Lim, Y.C.; Goh, P.S. Recent Progress of Ag/TiO₂ Photocatalyst for Wastewater Treatment: Doping, Co-Doping, and Green Materials Functionalization. *Appl. Mater. Today* **2022**, *27*, 101500. [[CrossRef](#)]
98. Nur, A.S.M.; Sultana, M.; Mondal, A.; Islam, S.; Robel, F.N.; Islam, A.; Sumi, M.S.A. A Review on the Development of Elemental and Codoped TiO₂ Photocatalysts for Enhanced Dye Degradation under UV-Vis Irradiation. *J. Water Process Eng.* **2022**, *47*, 102728. [[CrossRef](#)]
99. Laky, D. Predictive model for drinking water treatment technology design – the efficiency of arsenic removal by in-situ formed ferric-hydroxide. *Period. Polytech. Civ. Eng.* **2010**, *54*, 45. [[CrossRef](#)]
100. Tshukudu, T.; Zheng, H.; Yang, J. Optimization of Coagulation with PFS-PDADMAC Composite Coagulants Using the Response Surface Methodology Experimental Design Technique. *Water Environ. Res.* **2013**, *85*, 456–465. [[CrossRef](#)]
101. Corral Bobadilla, M.; Lorza, R.; Escribano García, E.; Somovilla Gómez, F.; Vergara González, E. Coagulation: Determination of Key Operating Parameters by Multi-Response Surface Methodology Using Desirability Functions. *Water* **2019**, *11*, 398. [[CrossRef](#)]